Journal of Mines, Metals and Fuels, *73(10): 3013-3034; 2025. DOI: 10.18311/jmmf/2025/49434*

Online ISSN : 0022-2755

Journal of Mines, Metals and Fuels

Contents available at: *www.informaticsjournals.co.in/index.php/jmmf*

Synthesis and Characterization of Monometallic and Bimetallic Nanoparticles Derived from *Parkia biglandulosa:* A Green Approach

Vaishali N. Patil[1], Ummar Pasha Shaik[2], Alka Sawaikar[1], Ashwin N. Bochare[1], Rahul Shivaji Yadav[3]*, Shobha Waghmare[4], Kiran Kokate[5], Pradip Tamkhade[3] and Suvarna Pawar[6]

[1]*Department of Engineering Sciences and Humanities, Marathwada Mitramandal's College of Engineering Pune - 411052, Maharashtra, India*

[2]*Department of Physics Anurag Engineering College, Ananthagiri, Suryapet - 508206, Telangana, India*

[3]*Department of Mechanical Engineering, Marathwada Mitramandal's College of Engineering, Karvenagar - 411052, Maharashtra, India; yahulyadav491@gmail.com*

[4]*Department of Chemistry MES abasaheb Garware College Pune - 411004, Maharashtra, India*

[5]*Dr. Vishwanath Karad, MIT World Peace University, Kothrud, Pune - 411037, Maharashtra, India*

[6]*Department of Computer Engineering, Sinhgad College of Engineering, Pune University, Pune - 411041, Maharashtra, India*

Abstract

The synthesis of nanoparticles was achieved through three main methods, viz. physical, biological and chemical. After studying the literature of all these methods, and also the harmful impact of chemical and physical methods, we opted for biological, i.e. green synthesis of monometallic nanoparticles and bimetallic nanoparticles. Various monometallic and bimetallic nanoparticles have been successfully synthesised and characterised using flower extract.

Major Findings: *Single and bimetallic nanomaterials were successfully synthesised using a green, sonochemical method with flower extract and characterised through various techniques. UV-Vis spectroscopy, XRD, SEM, TEM, and HRTEM confirmed properties like band gap, morphology, and bimetallic nature. These findings support their potential for future applications.*

Keywords: *Bimetallic Nanoparticles, Monometallic, Physical and Biological properties*

1.0 Introduction

Synthesis of nanomaterials by using a green approach is the main methodology followed in this work. The following are the details of the plant, and in this work, flowers are used for the reduction of metal salts to nanomaterials. The *Parkia* genus is a green tree distributed across the Neotropics, Asia and Africa. *Parkia biglandulosa,* this species has many medicinal applications such as diabetes, diarrhoea, hypertension, wound, cough, conjunctivitis and measles[1]. Phytochemical analysis shows the presence of secondary metabolites, phenolic compounds, flavonoids, terpenoids and many volatile compounds, etc. Their extracts show many antimicrobial activities, anticancer activities[2]. Flower extract of *Parkia biglandulosa* also has the same properties and compounds. In this work, flowers of *Parkia biglandulosa* have been used for the synthesis of single nanoparticles as well as bimetallic nanoparticles[3-11].

**Author for correspondence*

Figures 1 and 2 explain FTIR spectra and UV-Visible spectra of this flower powder, where one can see peaks for functional groups like carbonyl, hydroxyl, and amine frequency, which helps for the reduction of nanoparticles, which can be further stabilised. UV -visible spectra explain the presence of n to pi transition.

Botanical name: *Parkia biglandulosa*

Kingdom: Plantae Order: Fabaceae Family: *Mimosaceae*
Genus: Parkia
Species: Parkia biglandulosa
Common Name – Chenduful, Badminton ball Tree,
African Lotus tree



1.1 Synthesis of Nanomaterials by Using Flower Extract of *Parkia biglandulosa* (Chendul)

(i) Making of flower extract
Parkia biglandulosa, chenduful flowers were collected in February and March every year at Pune, Deccan area, near the roadside. These flowers were dried in the shade to preserve all phytochemicals, and then, the dried powder was used for the synthesis of nanomaterials.

(ii) 5 gm dried Flower powder taken in a beaker and 100 ml distilled water added to it. It is boiled and filtered till we get a clear extract. The filtrate was used as plant extract for the synthesis of monometallic and bimetallic nanoparticles by using sonochemical[3,4] methods.





Figure 1. Flower and tree of *Parkia biglandulosa*.

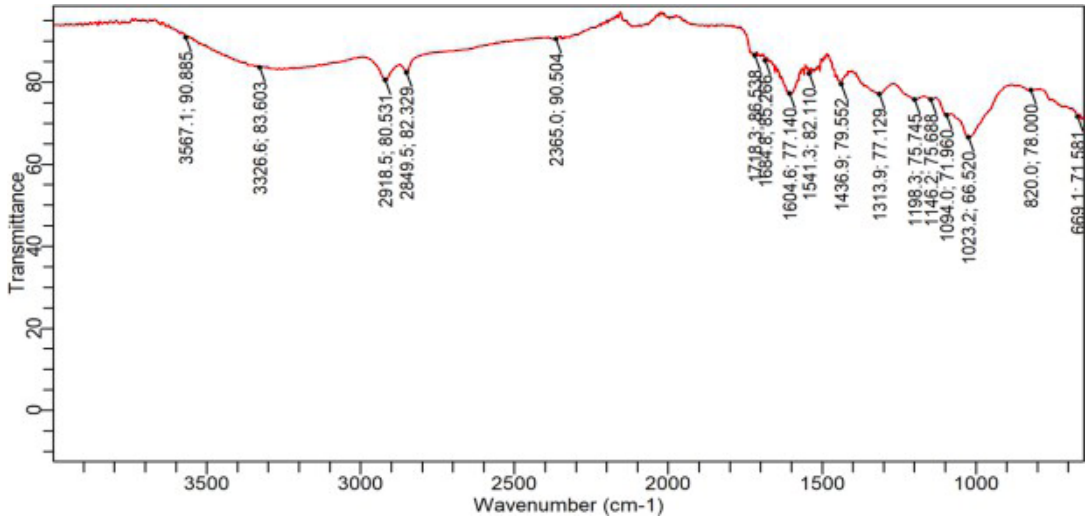


Figure 2. FTIR spectra of the flower powder of *Parkia biglandulosa.*

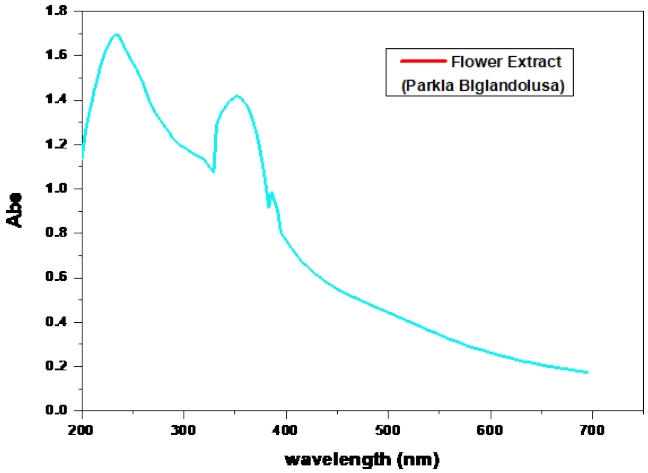


Figure 3. UV-Vis spectrum of Flower extract (*Parkia biglandulosa*).

1.2 Synthesis of Monometallic Nanoparticles

$FeSO_4$ $5H_2O$ (1m Mole (0.11 gm) metal salt was dissolved in 200 ml distilled water. 3ml flower extract was added to it. And then the solution is sonicated for 15 minutes kept for 24 hours. The next day iron nanoparticles formed were observed by using colour change and further characterisation. Formed monometallic iron nanoparticles were centrifuged at 4000 rpm and collected and dried, and used for further characterized techniques[12,13].

The following Table 1 shows metal salts used for single nanoparticle synthesis by using the above procedure for all.

Table 1. Bimetallic nanomaterial salt and concentration

Sr. No.	metals	Chemical (salt)
1	Cu	$Cu(NO_3)2$
2	Ni	$Ni(NO_3)2$
3	Ag	$AgNO_3$
4	Pd	$Pd(Cl)_2$
5	Ce	$CeCl_3.7H_2O$
6	Zn	$Zn(OAC)_2$
7	Ru	$RuCl_3.H_2O$
8	Y	YCl_3
9	Ti	$TiCl_3$
10	Co	$Co(NO_3)_2$
11	Fe	$FeSO_4.5H_2O$

1.2.1 Synthesis of Bimetallic Nanoparticles

Procedure – The Successive reduction method was followed for the synthesis of bimetallic nanoparticles. 1mM $FeSO_4$ $5H_2O$ (0.11 gm $FeSO_4$ is dissolved in 200 ml distilled water) and 3ml flower extract was added to it. And then the solution was sonicated for 15 minutes. After 24 hours, iron nanoparticles were formed. In the same solution, 1 mM $CuSO_4.5H_2O$ salt was added along with 5ml extract. And the resultant solution was sonicated and then kept for the next 24 hrs. After 24 hrs, formed bimetallic nanoparticles were centrifuged at 4000 rpm and collected and dried, and further characterised by using different techniques[14-20].

Table 2. Shows the combination of metal salts for bimetallic synthesis

Sr. No.	1st metal	Chemical (salt)	Molecular weight	mM	2nd metal	Chemical (salt)	Molecular weight	mM
1	Cu	$Cu(NO_3)_2$	241	1	Pd	$Pd(Cl)_2$	177.33	1
2	Ni	$Ni(NO_3)_2$	290	1	Pd	$Pd(Cl)_2$	177.33	1
3	Fe	$FeSO_4.7H_2O$	278.02	1	Ti	$TiCl_3$	154.22	1
4	Fe	$FeSO_4.7H_2O$	278.02	1	Zn	$Zn(OAC)_2$	219	1
5	Fe	$FeSO_4.7H_2O$	278.02	1	Ce	$CeCl_3.7H_2O$	372.60	1
6	Fe	$FeSO_4.7H_2O$	278.02	1	Y	YCl_3	195.26	1
7	Ni	$Ni(NO_3)_2$	290	1	Ru	$RuCl_3.H_2O$	207.43	1
8	Cu	$Cu(NO_3)_2$	241	1	Zn	$Zn(OAC)_2$	219	1
9	Ag	$AgNO_3$	169.87	1	Ti	$TiCl_3$	154.22	1
10	Fe	$FeSO_4.7H_2O$	278.02	1	Pd	$Pd(Cl)_2$	177.33	1
11	Ag	$AgNO_3$	169.87	1	Ni	$Ni(NO_3)_2$	290	1
12	Ag	$AgNO_3$	169.87	1	Y	YCl_3	195.26	1

1.3 Characterisation of Monometallic Nanoparticles and Bimetallic Nanomaterials

1.3.1 Characterisation by Using UV-Visible Spectroscopy

Table 3. UV-Vis spectra values of nanomaterials

Nanomaterials	Λmax1	OD1	Λmax2	OD2	Λmax3	OD3	Band gap. eV
Flower	234.94	1.69	354.13	1.41	387.58	0.9	
FeO	222.06	1.55	536.02	0.27			2.3
NiO	227.84	1.64	267.76	0.35	342.93	0.23	3.6
ZnO	229.38	1.66	312.37	0.50			3.9
Ag	203.16	0.97	417.96	0.35			2.9
Co	225.77	2.21	228.24	0.15			5.4
Ce	200.75	0.29	581.13	0.026			2.1
Ru	213.08	1.88	269.78	0.85	342.28	0.47	3.6
Ti	227.82	2.69	267.38	2.51	397.93	0.40	3.1
Pd	235.64	1.44	366.20	0.92	391.92	0.70	3.1
Fe-Ce	202.37	3.99	345.44	2.58	526.99	0.25	2.3
Fe-Cu	205.16	1.48	325.06	0.45			3.8
Fe-Zn	199.65	0.81	330.57	0.38			3.7
Fe-Ti	281.01	0.84					4.4
Ti-Ag	229.17	2.32	267.23	2.16			4.6
Zn-Cu	235.64	2.74	336.57	2.57	409.81	0.84	3.03
Ni-Ru	233.69	2.57	310.85	2.18	368.15	0.97	3.36

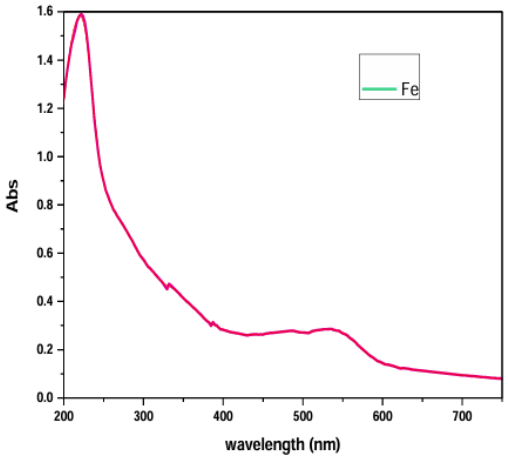


Figure 4. UV-Vis spectrum of Fe NP's.

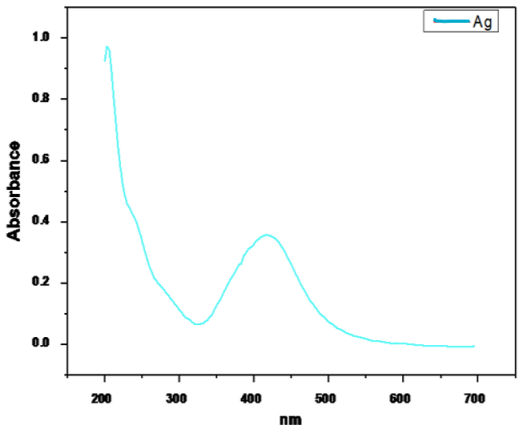


Figure 7. UV-Vis spectrum of Ag NP's.

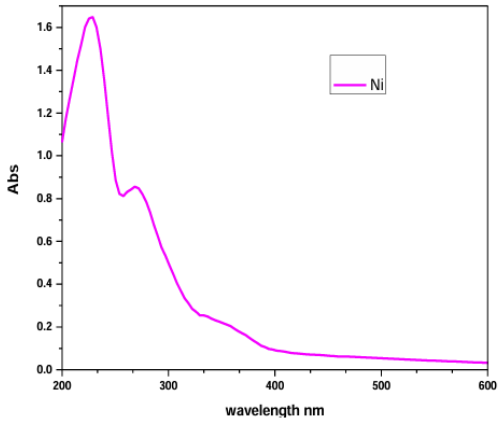


Figure 5. UV-Vis spectrum of Ni NP's.

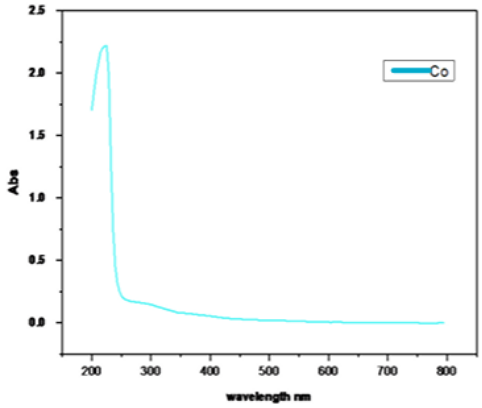


Figure 8. UV-Vis spectrum of Co NP's.

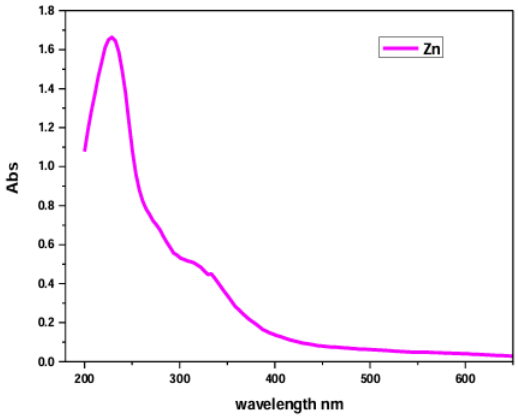


Figure 6. UV-Vis spectrum of Zn NP's.

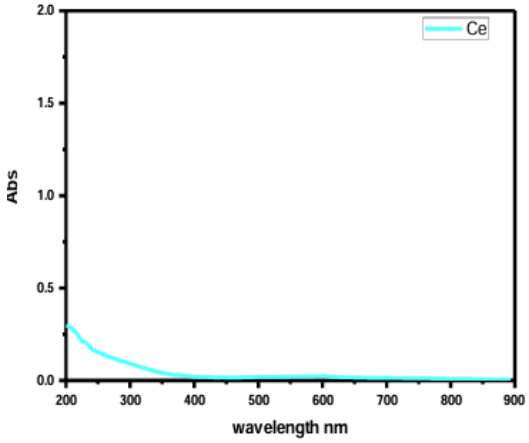


Figure 9. UV-Vis spectrum of Ce NP's.

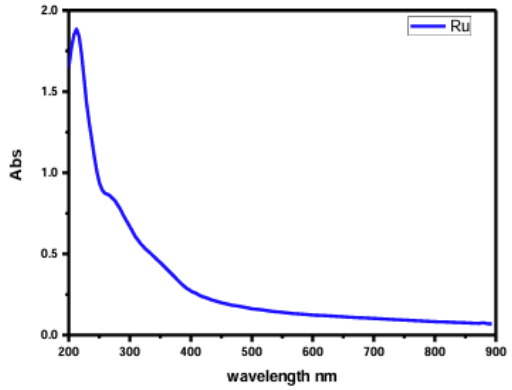


Figure 10. UV-Vis spectrum of Ru NP's.

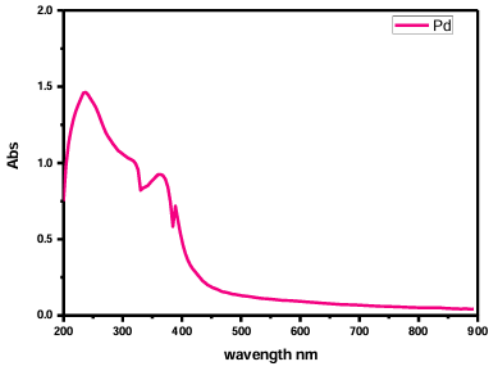


Figure 12. UV-Vis spectrum of Pd NP's.

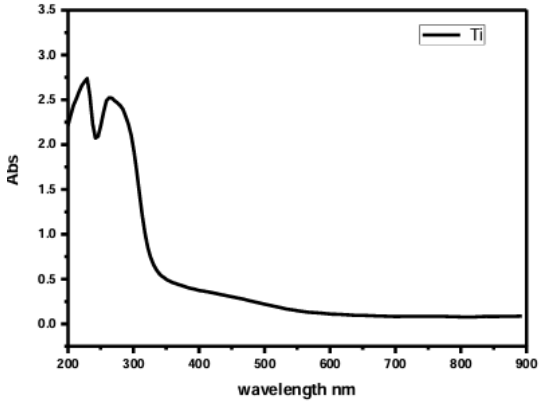


Figure 10. UV-Vis spectrum of Ti NP's.

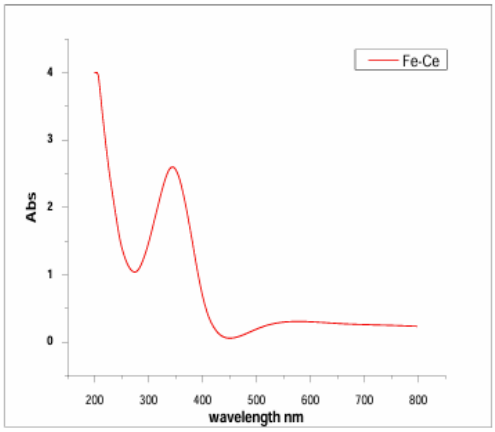


Figure 13. UV-Vis spectrum of Fe-Ce BMNM's.

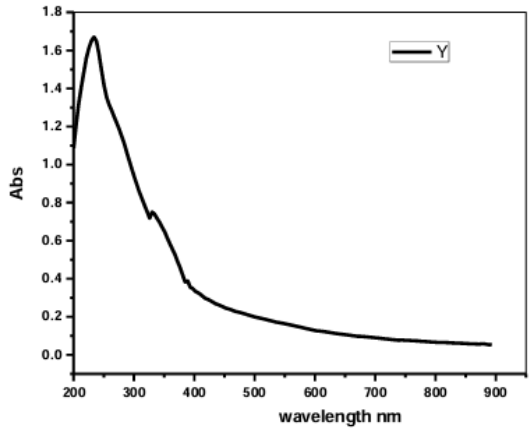


Figure 11. UV-Vis spectrum of Y NP's.

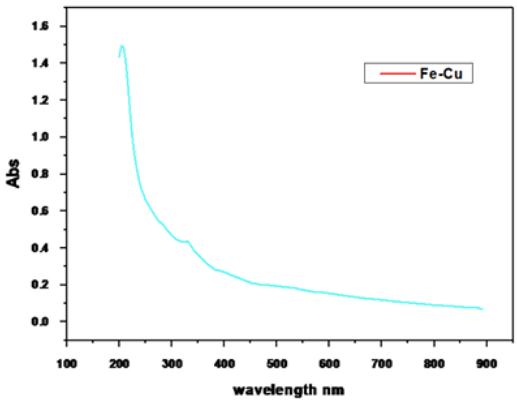


Figure 14. UV-Vis spectrum of Fe-Cu BMNM's.

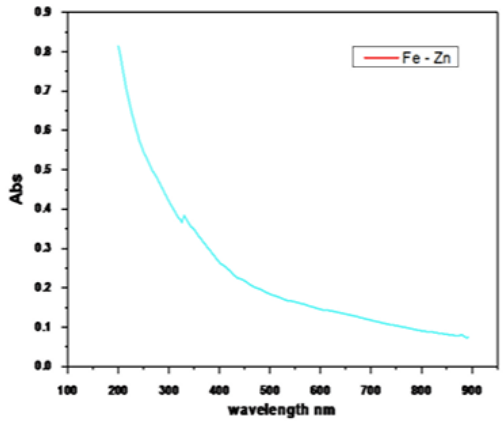


Figure 15. UV-Vis spectrum of Fe-Zn BMNM's

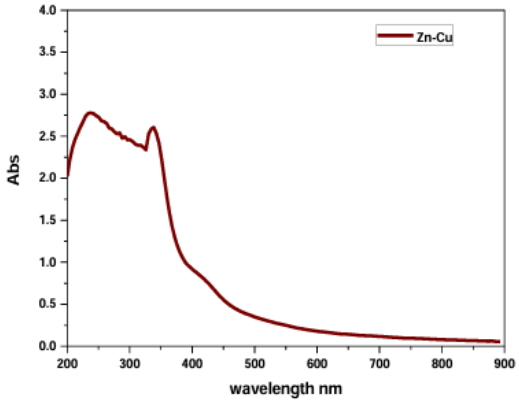


Figure 18. UV-Vis spectrum of Zn-Cu BMNM's.

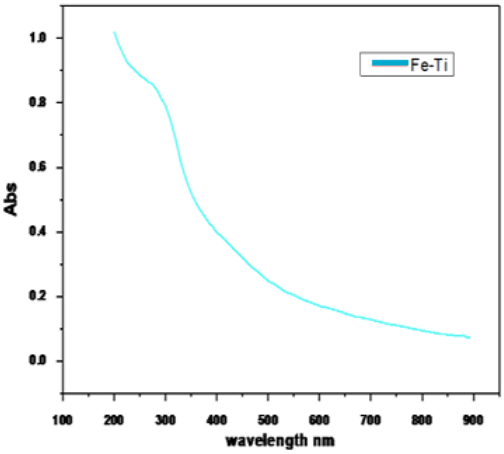


Figure 16. UV-Vis spectrum of Fe-Ti BMNM's.

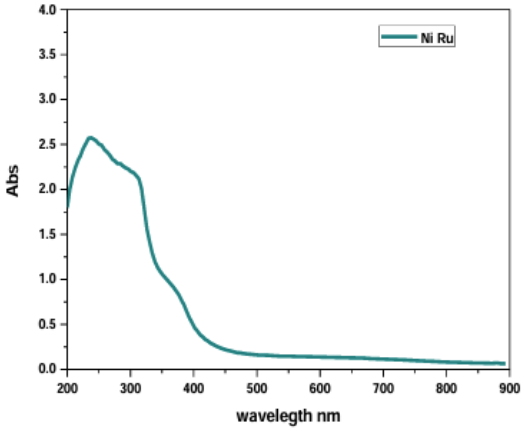


Figure 19. UV-Vis spectrum of Ni-Ru BMNM's.

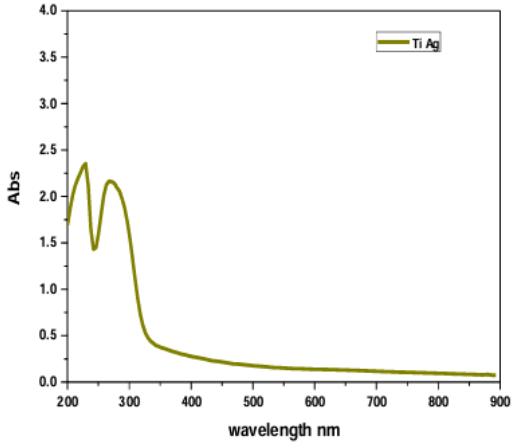


Figure 17. UV-Vis spectrum of Ti-Ag BMNM's.

2.0 Results and Discussion

2.1 UV-Visible Spectroscopy

UV-Visible spectra were done on a single-beam Systronic instrument and water as a solvent in our laboratory.

Table 2 shows UV-Visible data for single as well as bimetallic nanomaterials. Reduced metal nanoparticles were synthesised and characterised by using UV-Visible spectroscopy. Flower extract in this work shows three absorption bands, which can confirm certain organic moieties present in the extract. 234nm, 354nm, and 387nm readings show polyphenolic nature, and some other transitions are possible in this region. These components of flower extract work as reducing agents, capping agents, and stabilising agents.

For iron oxide nanoparticles, two absorption peaks are shown, which are explained at 222nm, its oxide peak and at 536nm it is iron III high-spin species in nano form.

For Nickel oxide nanoparticles characteristic peak is at 342nm. From this, one can calculate the band gap, which is 3.6 eV. ZnO shows UV-visible region spectra peak at 312nm, which is characteristic of zinc oxide, and it has a band gap of 3.9 eV.

Band gap increases with a decrease in size due to confinement of electrons at nano nanoscale, which is also called the quantum confinement effect. Silver colloidal solution shows a surface plasmon resonance peak at 417nm in the visible region. The cobalt oxide peak is in the UV region with a bandgap of 5.4 eV. CeO_2 nanoparticles have a very low bandgap of 2.1 eV at the 581nm region and are a type of semiconductor.

When iron is with CeO_2, then the visible range peak is retained at 527nm. All bimetallic nanomaterials are in oxide form, so all absorptions are in the UV region. Copper and Ruthenium will have Visible light region absorption like surface plasmon resonance.

2.1.1 Characterisation by Using FTIR Spectra

FTIR spectra of nanomaterials explain functional groups, which are intact with it after synthesis and drying, and which further help in application. The above plots 2.5a to 2.6h explain IR plots for single nanoparticles as well as bimetallic nanomaterials.

In single nanoparticles, the IR spectra of Fe and Ce show N H or OH stretch with all frequencies of natural polyphenols. In bimetallic, three stretching bands are prominent, which are shown in the bimetallic above plots

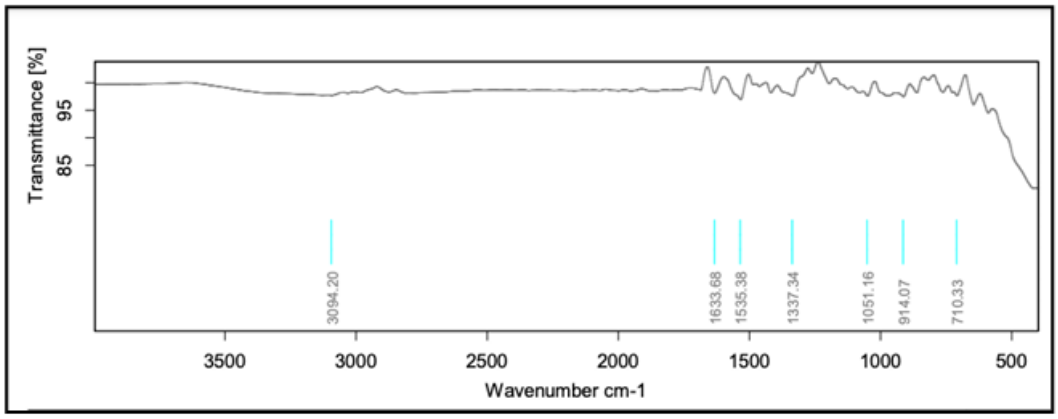


Figure 20. FTIR spectra of Agnp.

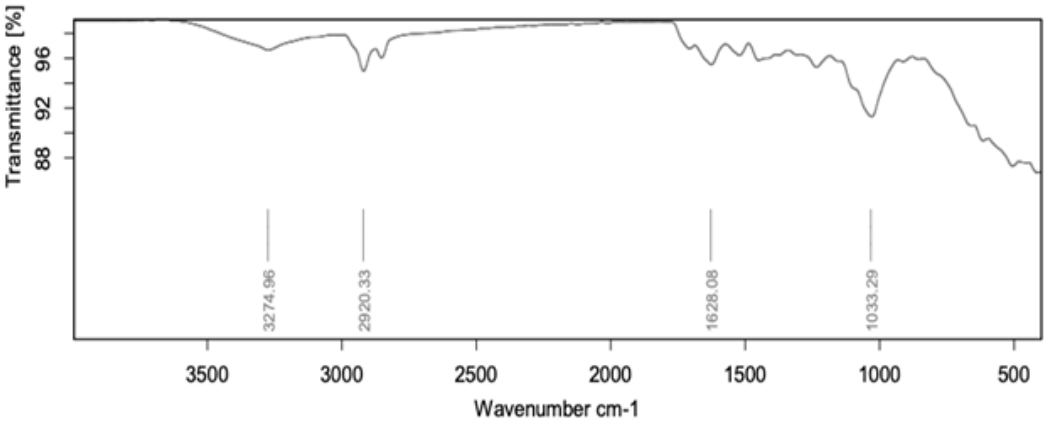


Figure 21. FT-IR spectra of Fe NP's.

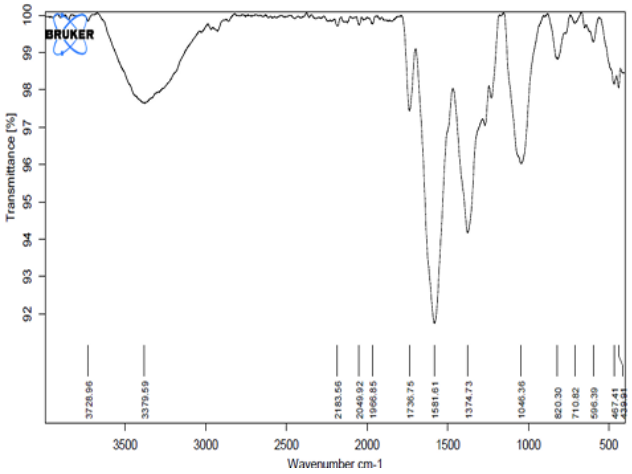


Figure 22. FT-IR spectra of Cu NP's.

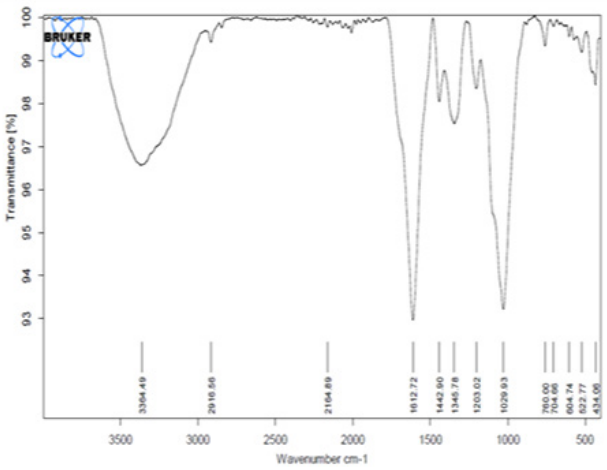


Figure 23. FT-IR spectra of Pd NP's.

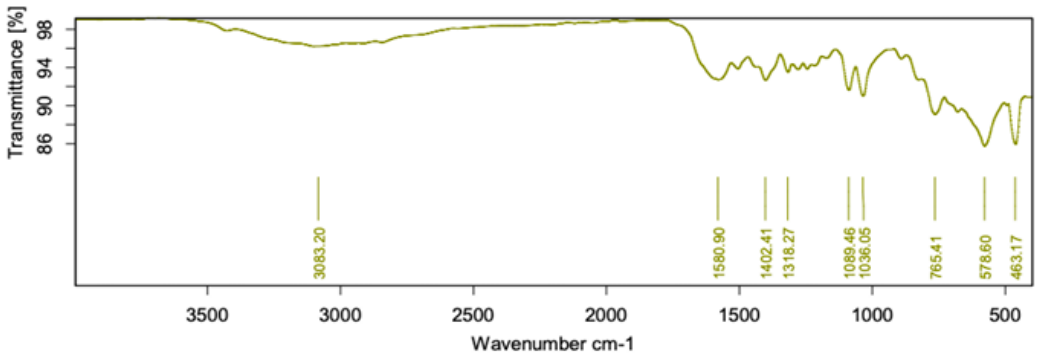


Figure 24. FT-IR spectra of Zn NP's.

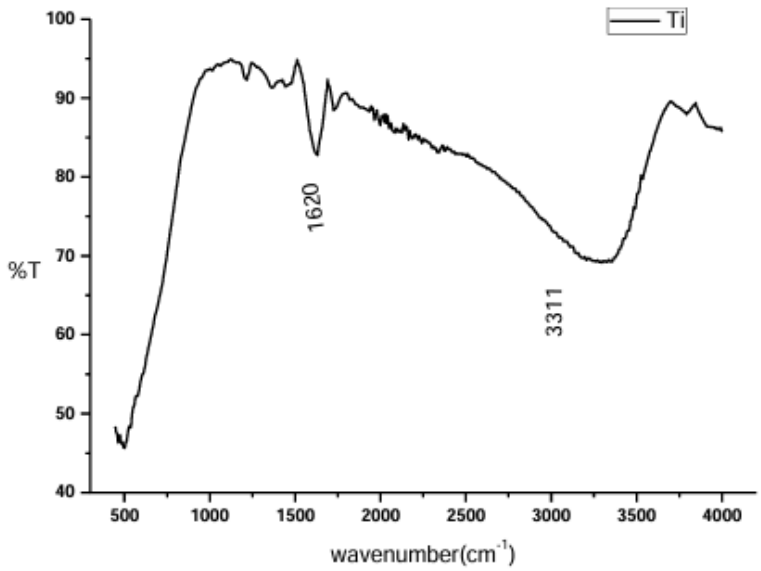


Figure 25. FT-IR spectra of Ti nanoparticles.

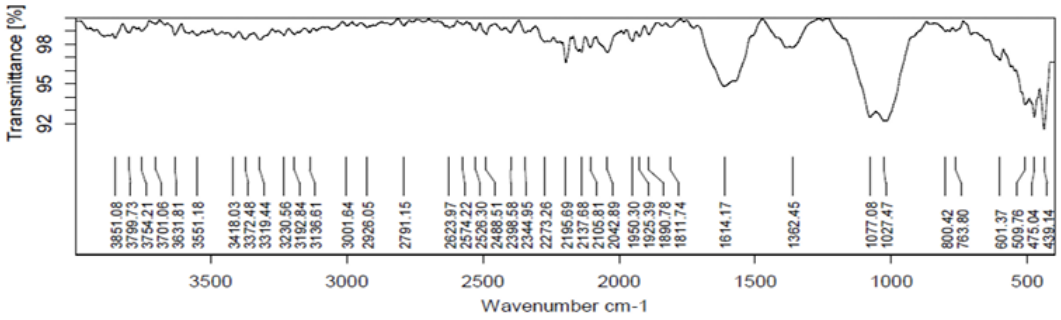


Figure 26. FT-IR spectra of Fe-Ce bimetallic nanomaterials.

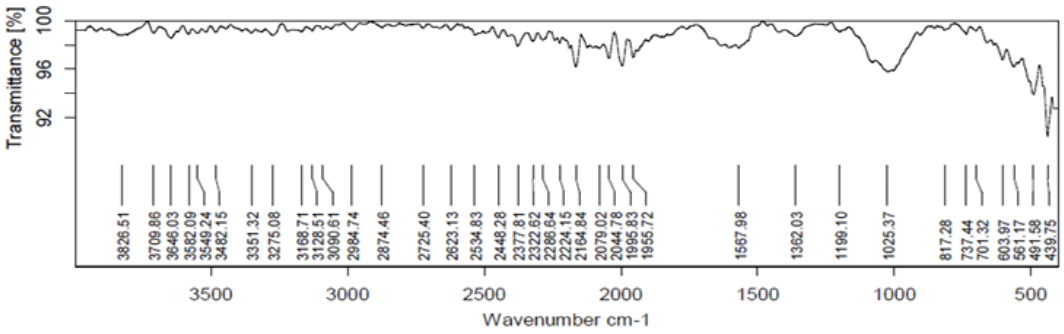


Figure 27. FT-IR spectra of Fe-Cu bimetallic nanomaterials.

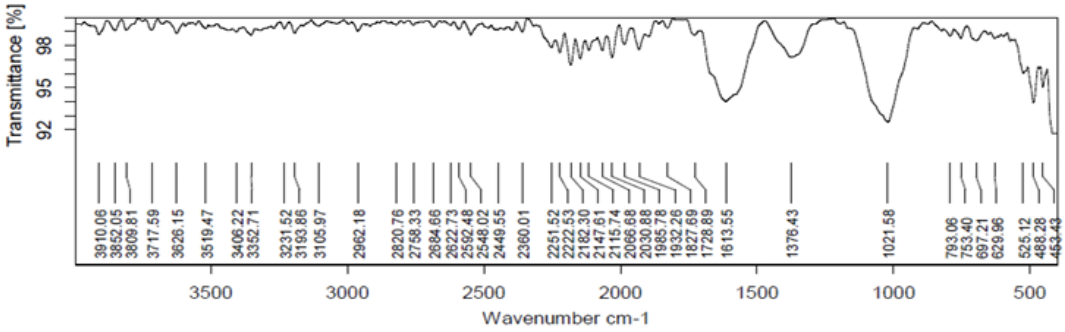


Figure 28. FT-IR spectra of Fe-Zn bimetallic nanomaterials.

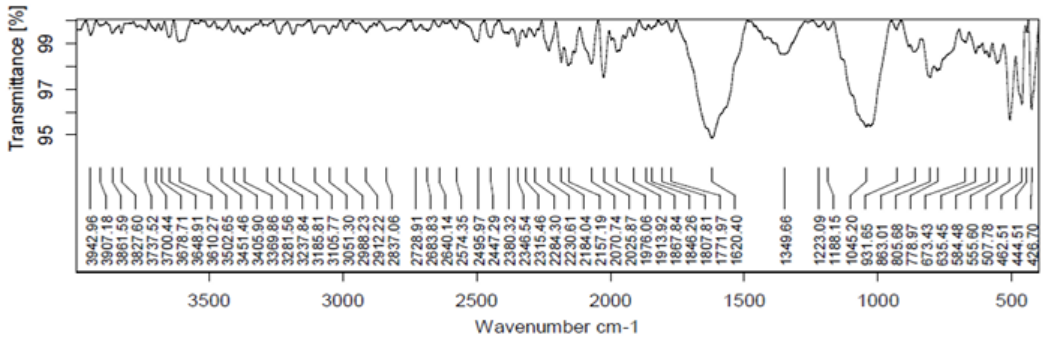


Figure 29. FT-IR spectra of Fe-Ti bimetallic nanomaterials.

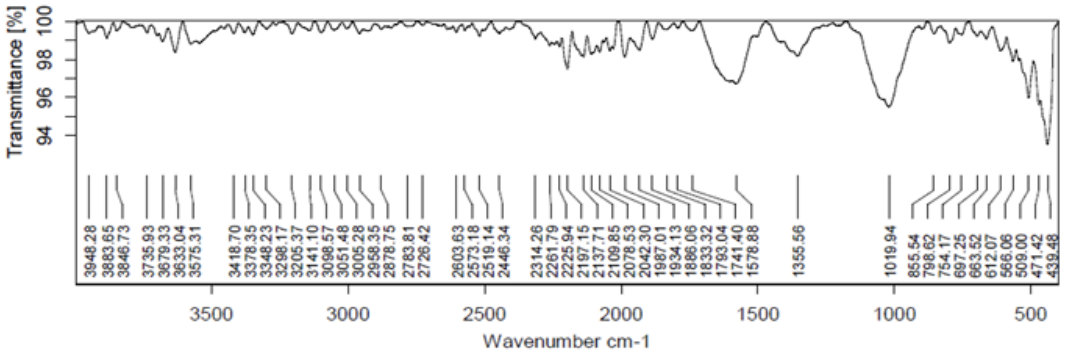


Figure 30. FT-IR spectra of Fe-Y bimetallic nanomaterials.

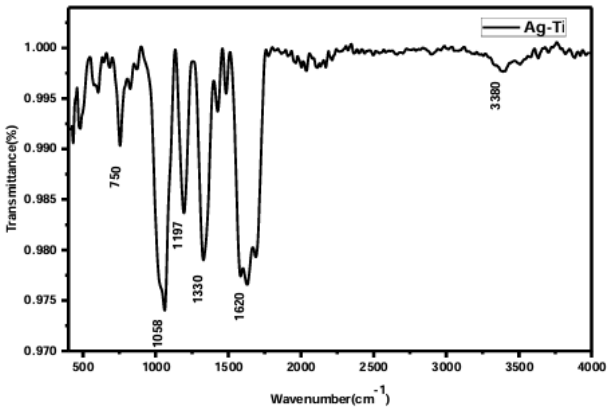


Figure 31. FT-IR spectra of Ag-Ti BMNM's.

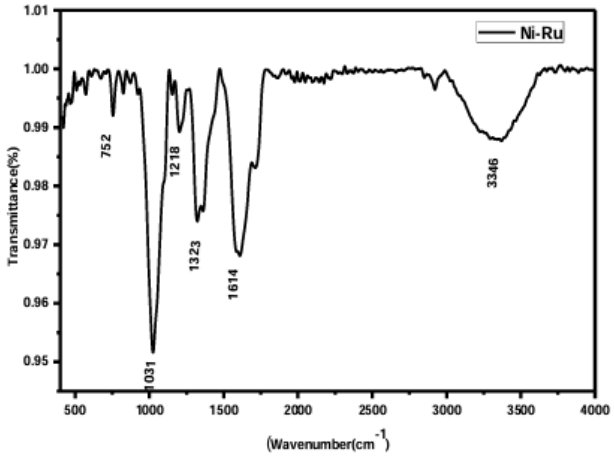


Figure 32. FT-IR spectra of Ni-Ru BMNM's.

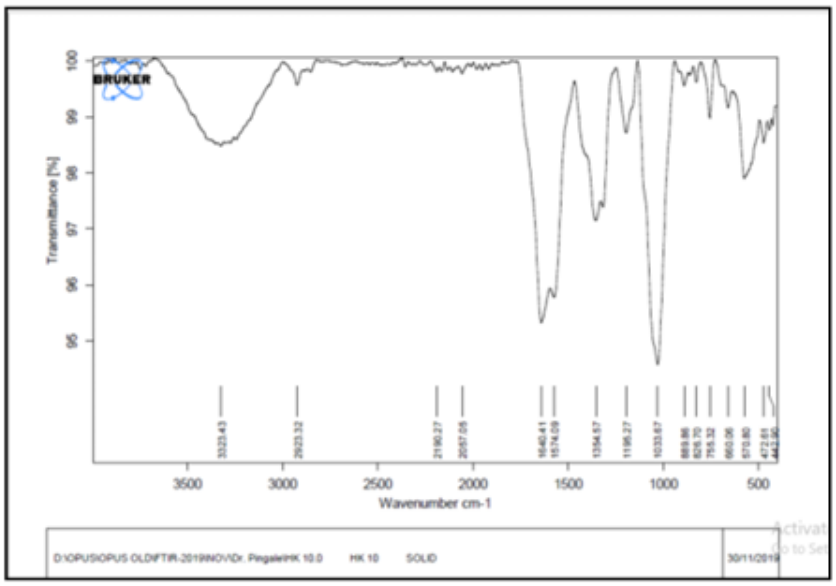


Figure 33. FT-IR spectra of Cu-Zn BMNM's.

around 1750cm^{-1}, 1360cm^{-1} and 1013cm^{-1}, which explains amide linkages with confirmation of polyphenolic nature of molecules with nanomaterials.

2.1.2 Characterisation by Using X-ray Diffraction

2.2 Powder X-ray Diffraction Spectroscopy

Fe_3O_4 – Figure 34 shows the Fe_3O_4 structure, and it matches with JCPDS file number-35-3107, and diffraction peaks 2q values are observed at 23.33^0, 28.47^0, 35.74^0, 46.51, 61.37^0, and 76.09^0, which match with the given JCPDS file. These 2q can be indexed planes to the (220), (311), (400), (422), (511), (440), and (533) of Fe_3O_4, which shows cubic structural phase respectively.

CeO_2 – Figure 35 shows CeO_2 nanoparticles, which match with JCPDS file number 43- 1002, with diffraction peaks at 2q values observed at 28.5^0, 33.9^0, 47.8^0, 56.2^0, 58.5^{0,} and 69.10^0, which correspond to (111), (200), (220), (311), (222), and (400) broad peaks due to the small size of ceria nanoparticles.

ZnO- Figures show XRD of ZnO nanoparticles and peaks were observed at 29^0, 32.97^0, 34.98^0, 49.65^0, 58.55^0 and 69.20^0, which are indexed as (100), (002), (101), (102), (201) and (202).

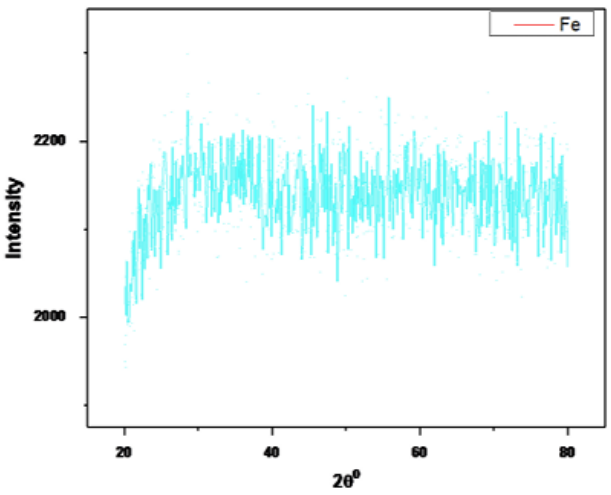


Figure 34. X-ray diffraction pattern of Fe NP's.

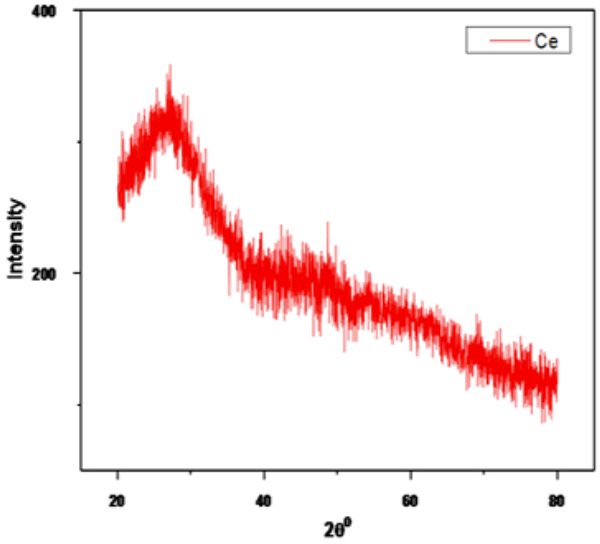


Figure 35. X-ray diffraction pattern of Ce NP's.

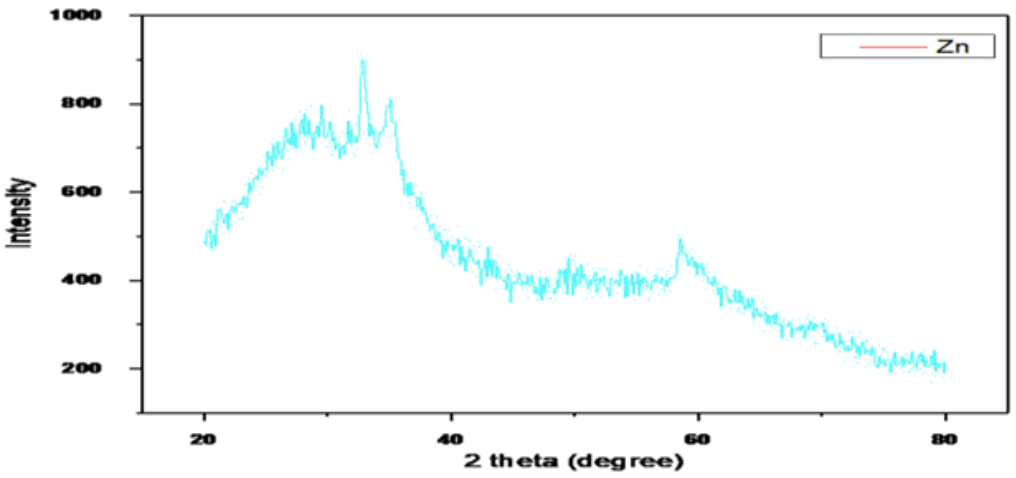


Figure 36. X-ray diffraction pattern of Zn NP's.

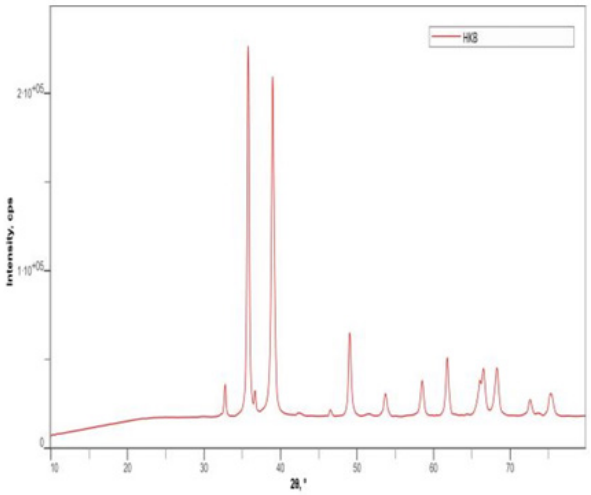


Figure 37. X-ray diffraction pattern of CuO NP's

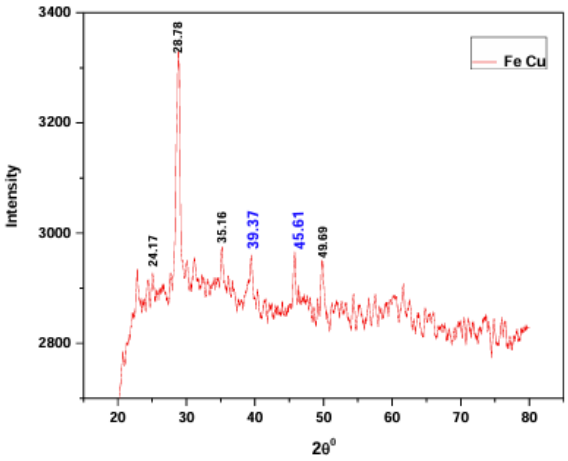


Figure 39. X-ray diffraction pattern of Fe-Cu BMNM's.

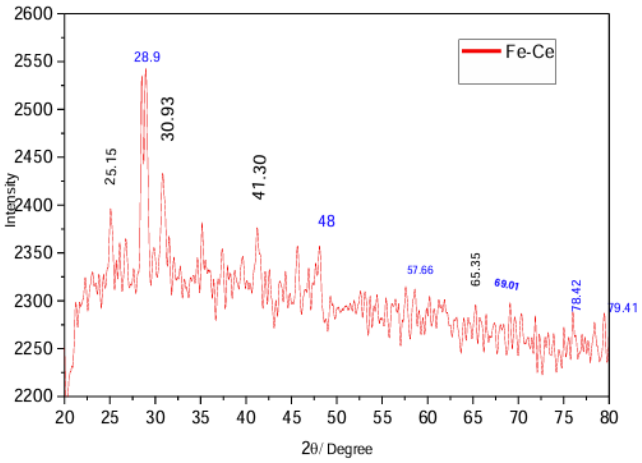


Figure 38. X-ray diffraction pattern of Fe-Ce BMNM's.

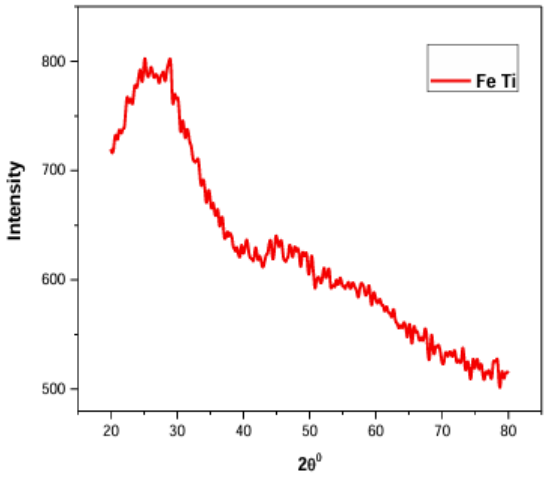


Figure 40. X-ray diffraction pattern of Fe-Ti BMNM's.

Table 4. X-ray diffraction 2Θ values of nanomaterials

Nanomaterial	2θ values								
Fe	23.33	28.47	35.74	46.51	61.37	76.09			
Ce	20.83	27.08	36.95	49.07	69.22	74.48			
Zn	29	32.97	34.98	49.65	58.55	69.20			
Cu	21.45	26.93	38.24	40.38	43.38	55.91			
Fe-Ce	25.15	28.9	30.93	41.30	48	57.66	65.35	69.27	75.93
Fe-Zn	24.05	28.38	31.23	34.62	40.18	46.69	52.26	58.64	67.46
Fe-Ti	25.12	29.05	44.94	50.36	55.18	67.61	73.16	78.45	
Fe-Cu	24.17	28.78	35.16	39.37	45.18	49.69	61.45		
Fe-Y	22.48	28.70	43.09	53.14	60.80	63.18	71.77	74.94	

These peaks are matched with (JCPDS-36-1451) data card and average crystal size by using the Debye Scherrer equation, D = (kλ/β cos θ) CuO- Figures show XRD of CuO -The peak positions of 2q are 32.6. 35.6. 38.9. 49. 54. 59. 62.5. 67. 68. 73. 75, which are indexed as (110), (-111), (111), (-202), (020), (202), (-113), (-311), (220), (311) and (004) obtained from the International Centre of Diffraction Data card (JCPDS-80-1916), which conforms formation of monoclinic CuO nanoparticles. The crystallite size of CuO nanoparticles by using the Debye-Scherrer equation is 28.6nm.

Bimetallic nanomaterials powder XRD spectra are shown as follows-

Fe_3O_4 at CeO_2 XRD spectra show prominent peaks of Fe_3O_4 and CeO_2 at 35.74^0 and $28.5^{0,}$ respectively, from XRD[18] spectra of 2q values, which confirms the formation of bimetallic **Fe_3O_4 at CeO_2**.

Fe3O4 at CuO bimetallic nanomaterial spectra shows 2q values at 35.16^0 and for CuO, 2q values show at $28.78^{0,}$ respectively, from the XRD spectra.

Fe_3O_4 at TiO_2 bimetallic nanomaterial spectra shows 2q values at 29.05^0 for **Fe_3O_4 and** 2q for TiO_2, it shows 44.94^0 respectively from XRD spectra.

Fe_3O_4 at ZnO bimetallic nanomaterial XRD spectra show 34.62^0 for Fe_3O_4 and 31.23^0 2q values for ZnO, respectively, from XRD spectra.

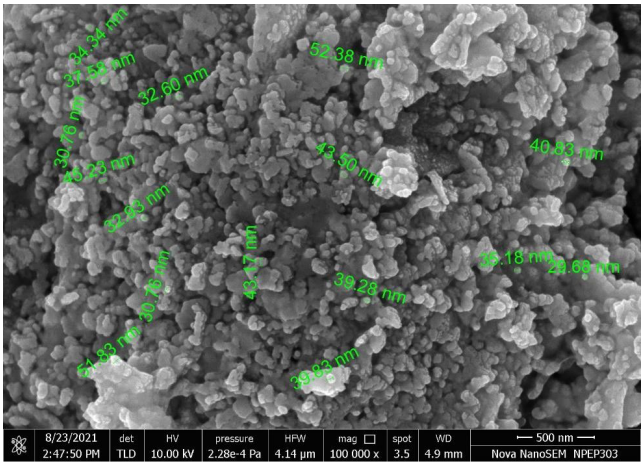


Figure 41. SEM images of Fe-Ce BMNM's.

Characterisation by using SEM *Images*

2.2 Scanning Electron Microscope (SEM)

Recently, Nanotechnology and nanoscience have provided high-resolution microscopy techniques that will explain or probe the objects at a very low scale, which require high-energy electrons. SEM is scanning electron microscopy[19], which shows surface imaging with resolution of small-sized particles, size distribution, and surface morphology with the shape of nanomaterials. By counting several particles, one can prepare a histogram

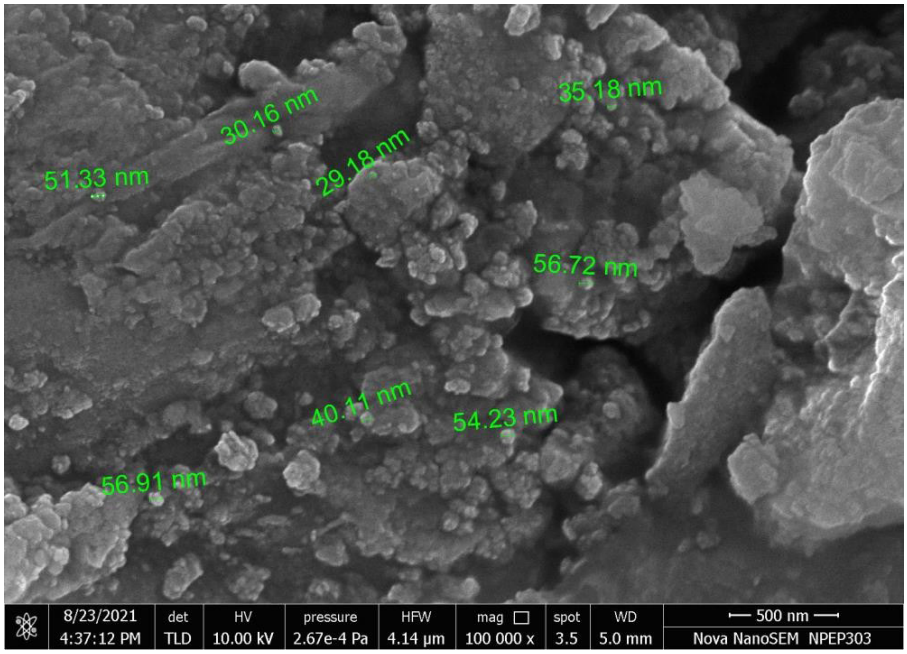


Figure 42. SEM images of Fe-Zn bimetallic nanomaterials.

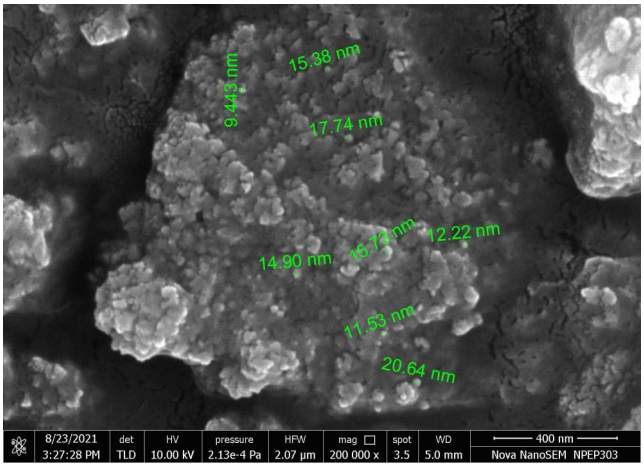


Figure 43. SEM images of Fe-Ti bimetallic nanomaterials.

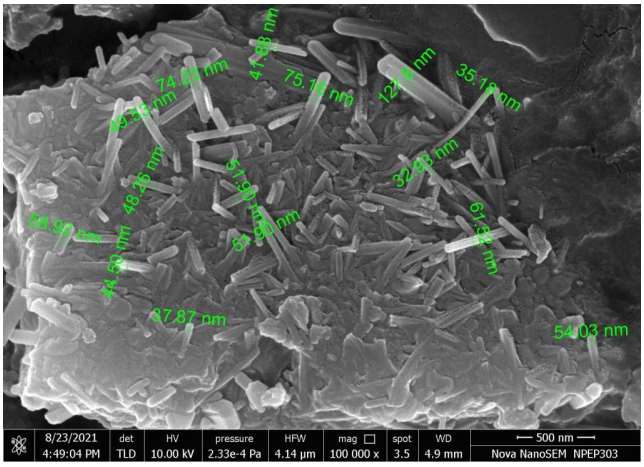


Figure 45. SEM images of Fe-Cu bimetallic nanomaterials.

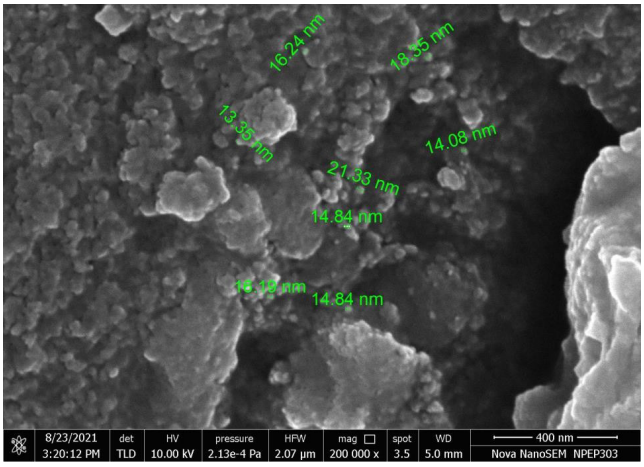


Figure 44. SEM images of Fe-Y bimetallic nanomaterials.

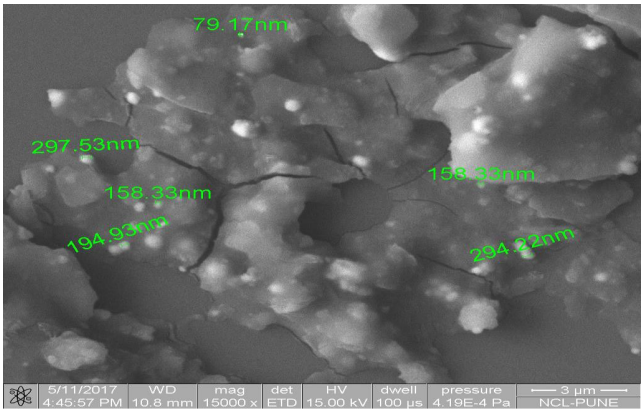


Figure 46. SEM images of Cu-Ni bimetallic nanomaterials.

Table 5. SEM values for monometallic and bimetallic nanomaterials

Nanomaterial	Size in nm								
Fe-Ce	34.34	32.60	43.50	39.28	35.18	40.83	32.93	30.76	51.83
Fe-Zn	51.33	30.16	29.18	35.18	56.72	40.11	54.23	56.97	
Fe-Ti	14.90	11.53	20.64	12.22	15.38	15.73	9.44		
Fe-Y	13.35	16.19	14.84	21.33	18.30	14.08	16.24		18.35
Fe-Cu	74.23	41.88	75.16	35.18	32.93	61.52	54.03	44.50	58.92
Cu-Ni	194.93	294.22	158.33		297.53				

of the size distribution of nanomaterials also explains the degree of particle aggregation and size of nanomaterials up to the 10nm scale.

From the Figures, all bimetallic nanomaterials are listed with size distribution and all morphological structural images. Except Fe-Cu bimetallic structure, all show aggregation of both the nanoparticles, but on a nanometre scale. If we look at the close size distribution, one can distribute particles into two broad size distributions, which confirms the bimodal nature of these nanomaterials. Fe-Cu shows a rod-like structure with polydispersed rods with a size distribution from

40nm to 75nm rod size whereas other bimetallic particles have a cubic to spherical nature. Fe-Ce shows a 30nm scale to 50nm scale particle distribution. Fe-Zn shoes 29nm to 57nm particle size, where a polydispersed nature of bimetallic nanomaterials. Fe-Ti particles are with a 9nm to 20nm scale, which are the smallest particles that have been synthesised by a green approach. Fe-Y is 14 nm to 21nm in size with a polydisperse nature. Cu -Ni are with a slightly higher size range from 158nm to 300nm.

2.2.1 Characterisation by Using HRTEM Images

The above HRTEM images confirm the bimetallic nature of nanomaterials by using the green synthesis method

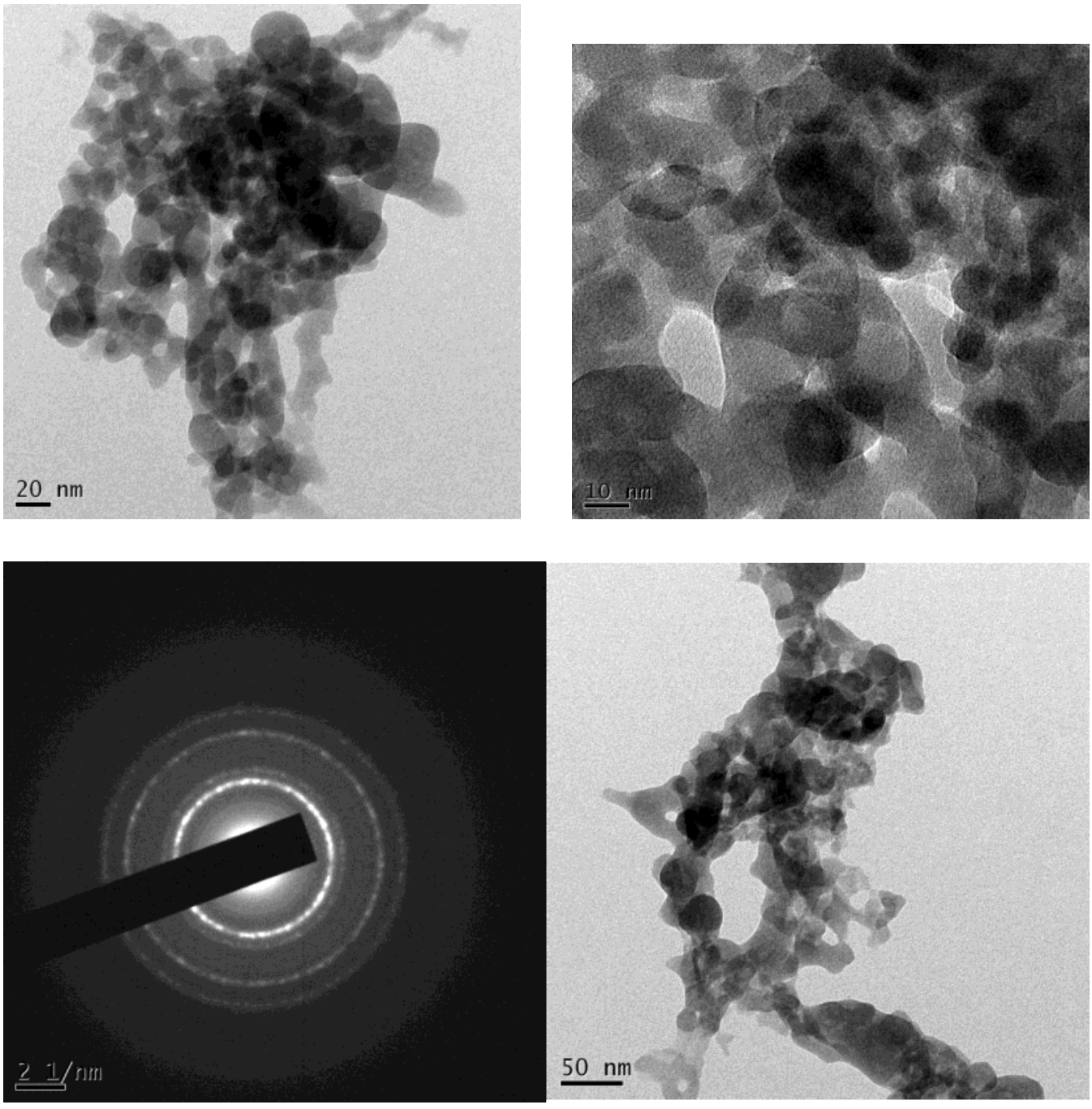


Figure 47. HRTEM of Fe@Y_2O_3 bimetallic nanomaterials.

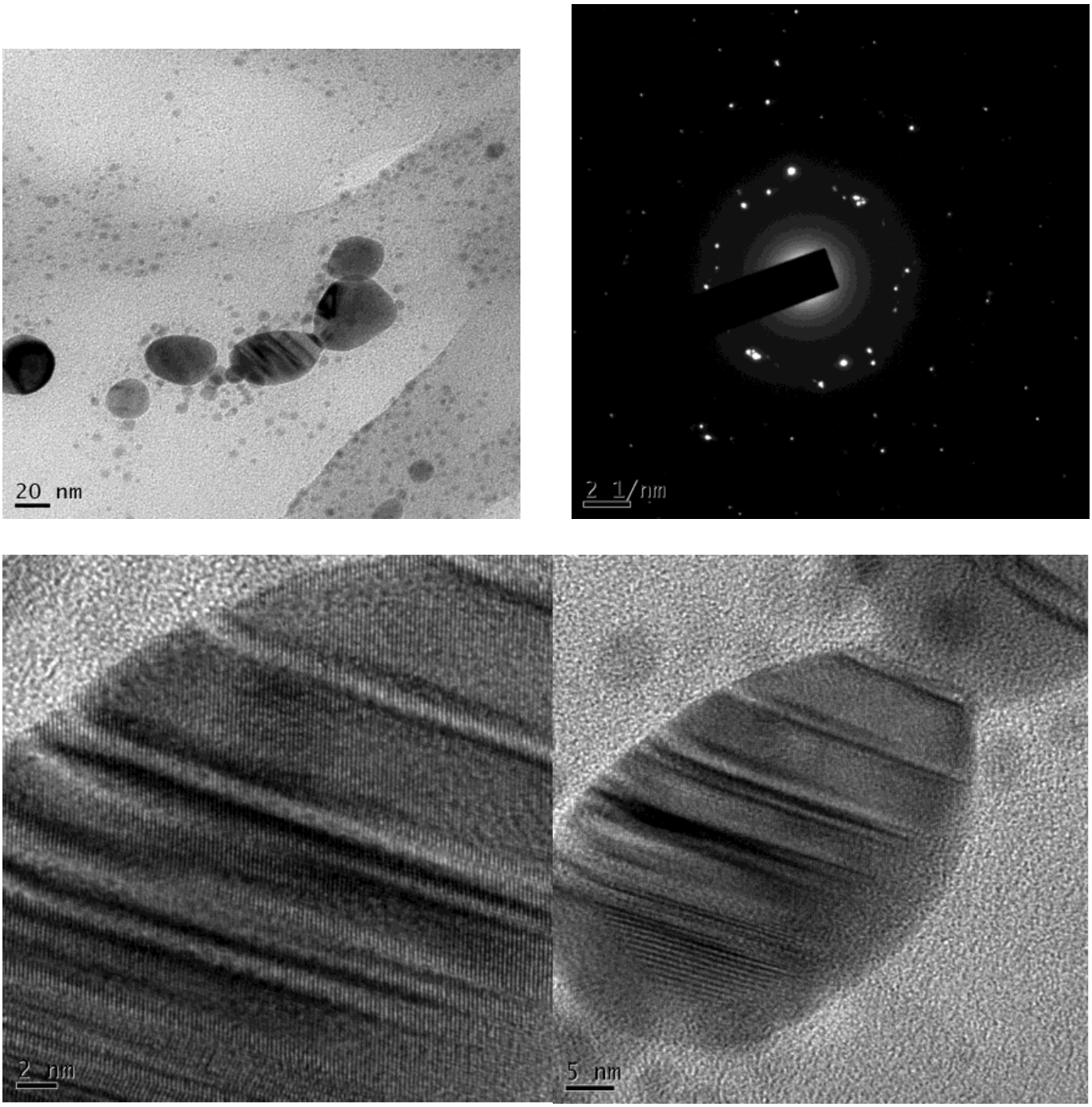


Figure 48. HRTEM images of silver bimetallic nanomaterials.

for different combinations of elements from the periodic table. Some are rod-like, spherical, and have a second metal as a shell on that structure.

2.2.2 Characterisation by Thermogravimetric Analysis

2.2.3 Thermogravimetric Analysis (TGA)

TG analysis 20 was done for bimetallic nanomaterials, which explains the thermal stability of these molecules. Table No. 2.5 shows the steps involved during the decomposition of the bimetallic nanomaterials. Fe-Cu, Ag-Ti, and Fe-Ce show two-step decomposition, and

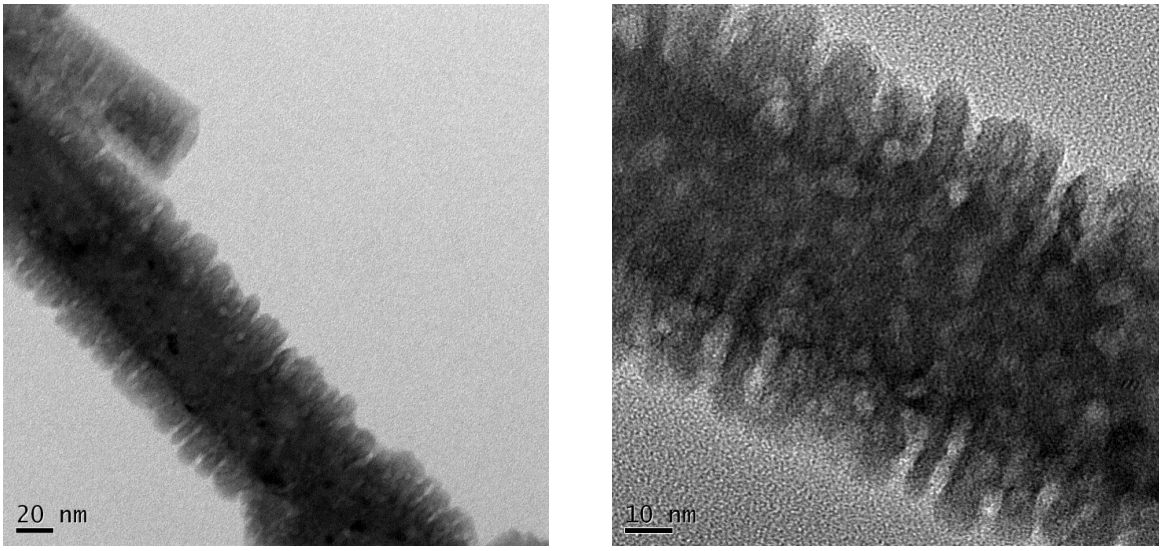


Figure 49. HRTEM images of bimetallic CuZn nanomaterials.

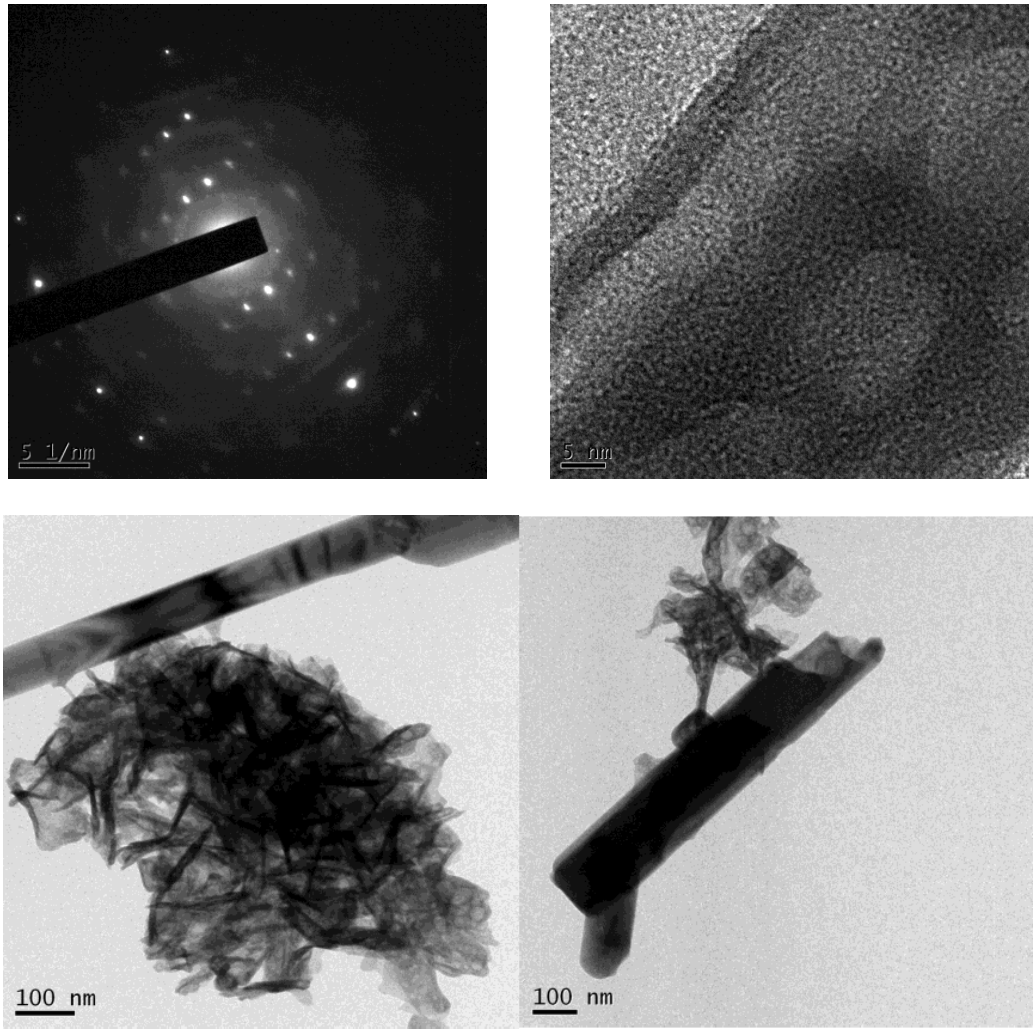


Figure 50. HRTEM images of bimetallic nanomaterials.

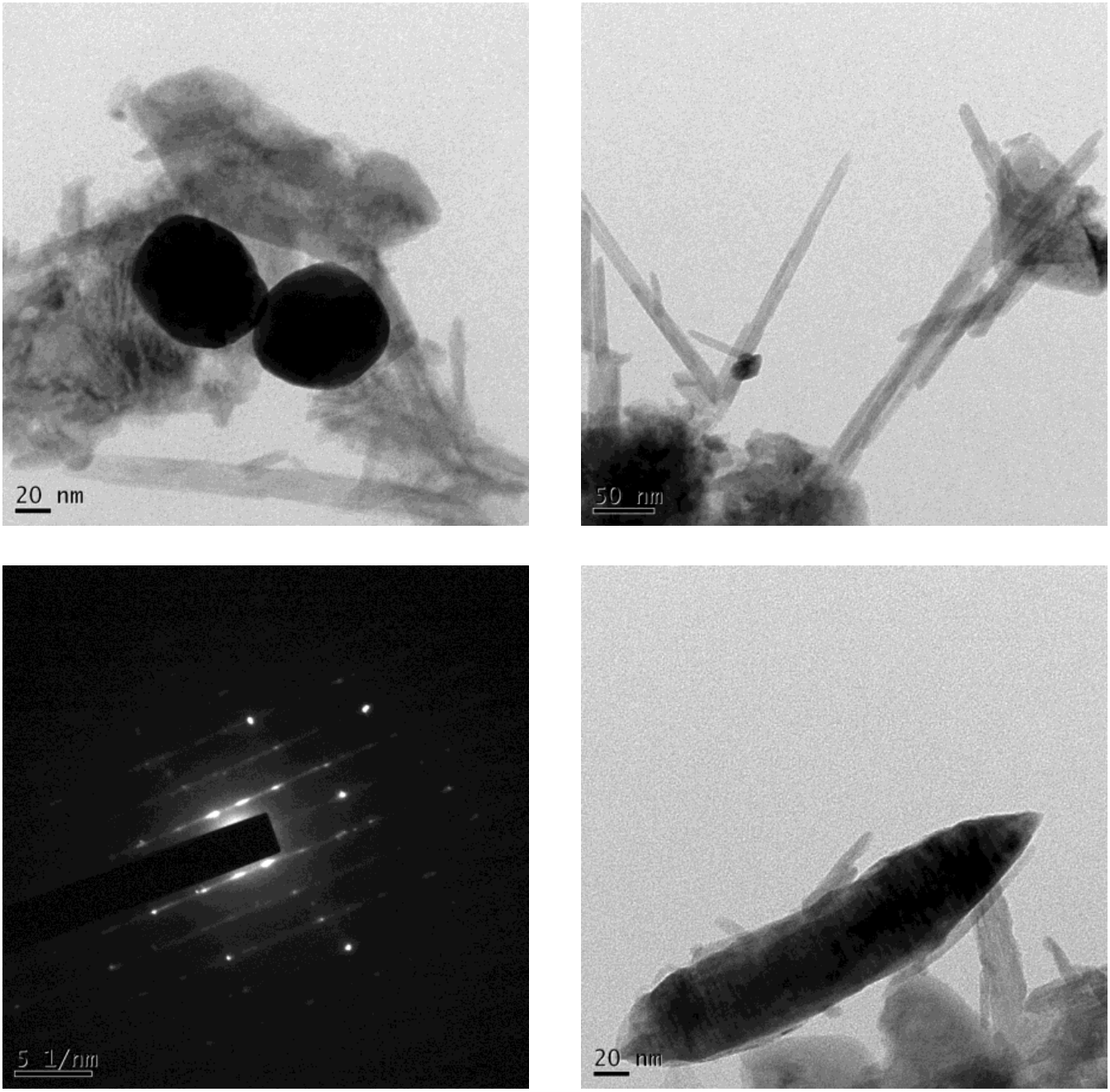


Figure 51. HRTEM images of bimetallic nanomaterials.

Ni-Ru and Cu-Zn show three-step decomposition. The thermal stability of bimetallic nanomaterials varies with metal combination. With Fe and other metals, it decomposes below 100°C. Other bimetallic nanomaterials have good stability, for example, Ag-Ti has 132°C. Ni-Ru has 150 °C and Cu-Zn has 186°C. Overall stability for these bimetallic nanomaterials is good for further application. Finally, all gets converted into the oxide form of the materials.

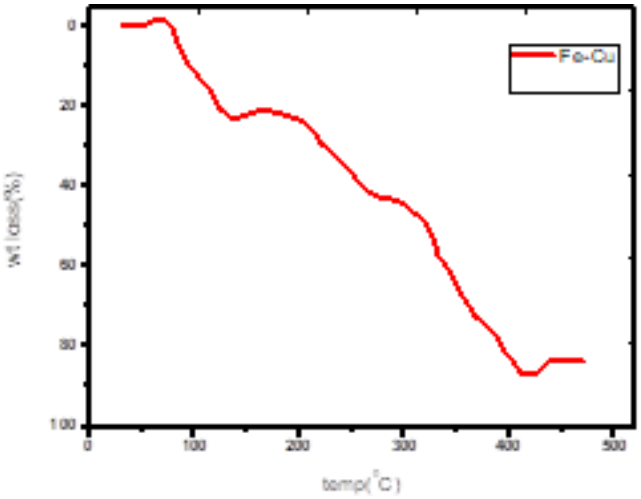


Figure 52. TGA analysis of Fe-Cu bimetallic nanomaterials.

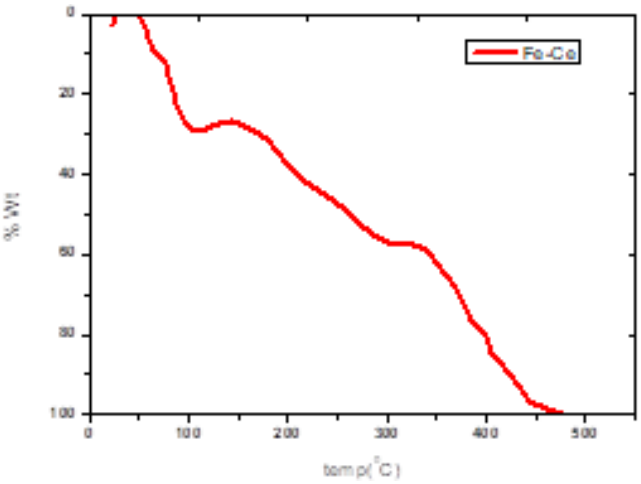


Figure 53. TGA analysis of Fe-Ce bimetallic nanomaterials.

Figure 54. TGA analysis of Ni-Ru bimetallic nanomaterials.

Figure 55. TGA analysis of Ag-Ti bimetallic nanomaterials.

Figure 56. TGA analysis of Cu-Zn bimetallic nanomaterials.

3.0 Conclusion

Successfully synthesised single as well as bimetallic nanomaterials by using flower extract and characterised by using various techniques. HRTEM explains the bimetallic nature, which will help in further work applications. The synthesis of single metal nanoparticles has been done successfully, and also for bimetallic synthesis by using a green approach and a sonochemical method, which is cheaper and follows green chemistry principles. These monometallic and bimetallic nanomaterials were well characterised by UV-Visible spectroscopy, which explains band gap and size correlation. Powder X-ray diffraction pattern, which explains the standard JCPDS file for specific nanomaterials. SEM images, i.e.,

Table 6. TGA values for monometallic and bimetallic nanomaterials

Sr. No.	Name	Temp(°C)	Weight loss (%)	Temp(°C)	Weight loss (%)
1	Fe-Cu	69	1.75	163	20.7
		291	42	443	84
2	Ag-Ti	132	0.15	302	25
		478	59	584	90
3	Ni-Ru	150	0.11	286	22
		444	48	472	76
		582	76		
4	Cu-Zn	186	1.7	357	25
		357	26	768	84
		801	84		
5	Fe-Ce	99	30	150	32
		325	62	450	94

scanning electron microscopy, explain morphology, size distribution, and geometry of the particles. TEM images explain the quantum dot nature of two bimetallic nanomaterials. HRTEM images confirm the bimetallic nature of nanomaterials, which have been discussed in the article.

4.0 References

1. Emam HE. Accessibility of green synthesised nanopalladium in water treatment. Results in Engineering. 2022; 15:100500. https://doi.org/10.1016/j.rineng.2022.100500
2. Mazhar T, Shrivastava V, Tomar RS. Green synthesis of bimetallic nanoparticles and their applications: a review. J Pharm Sci and Res. 2017; 9(2):102-110.
3. Sharma G, Kumar A, Sharma S, Naushad M, Dwivedi RP, AlOthman ZA, Mola H. Novel development of nanoparticles to bimetallic nanoparticles and their composites: A review. J King Saud Univ Sci. 2017; 29(1):50-68. https://doi.org/10.1016/j.jksus.2016.04.013
4. Anandan S, Ashokkumar M. Sonochemical synthesis of noble monometallic and bimetallic nanoparticles for catalytic applications. Cavitation. 2014; 55-88.
5. Ijaz I, Bukhari A, Gilani E, Nazir A, Zain H, Saeed R, Hussain S, Hussain T, Bukhari A, Naseer Y, Aftab R. Green synthesis of silver nanoparticles using different plant parts and biological organisms, characterisation and antibacterial activity. Environ Nanotechnol Monit Manag. 2022; 18:100704. https://doi.org/10.1016/j.enmm.2022.100704
6. Kalyankar VK, Dagade PM, Dagade SP, Waghmode SA. Biosynthesis of Silver nanoparticles using isolated superoxide dismutase enzyme from novel source *Papaverum somniferum* L. Res J Chem Environ. 2015; 19(3):77-80.
7. Pawar O, Deshpande N, Dagade S, Nigam-Joshie P, Waghmode S. Green synthesis of silver nanoparticles from purple acid phosphatase apo-enzyme isolated from a new source, *Limonia acidissima*. J Exp Nanoscience. 2015; 10(3):352-364. https://doi.org/10.1080/17458080.2015.1025300
8. Nigam P, Waghmode S, Louis M, Wangnoo S, Chavan P, Sarkar D. Graphene quantum dots conjugated albumin nanoparticles for targeted drug delivery and imaging of pancreatic cancer. J Mater Chem B. 2014; 2(22):3190-3195. https://doi.org/10.1039/C4TB00015C
9. Nigam P, Waghmode S, Sarkar D. Aptamer functionalized multifunctional fluorescent nanotheranostic platform for pancreatic cancer. J Nanopharmaceutics Drug Deliv. 2014; 2(4):280-287. https://doi.org/10.1166/jnd.2014.1070
10. Shete S, Shende S, Bhagwat K, Dagade S, Deshpande N, Waghmode S. Green synthesis of silver chloride nanoparticles by using *Rosa macdub* petal extract. Int J Biosci Nanoscience. 2014; 1(5):96-99.
11. Mane V, Lalaso M, Waghmode S, Jadhav KD, Dongare MK, Dagade SP. Nitration of benzene using mixed oxide catalyst. IOSR J Appl Chem. 2014; 7(7):50-57. e-ISSN: 2278-5736.
12. Mane VB, Chavan SP, Sayyad RJ, Deshmukh JM, Waghmode SA, Dagade SP. One-pot synthesis of benzimidazole derivatives by using solid acid catalysts at RT. Bionano Front. 2015; 6(2):123-131.

13. Alegaonkar APA, Kumar A, Alegaonkar PS, Waghmode SA, Pardeshi SK. Exchange interaction of itinerant electron donors of tetrakis (dimethyl amino) ethylene with localised electrons in graphene. Synthesis React Inorg, Metalorg Nano-etal Chem. 2014; 44(10):1081-1088. https://doi.org/10.1080/15533174.2013.817421
14. Waghmode S, Chavan P, Kalyankar V, Dagade SP. Synthesis of silver nanoparticles using *Triticum aestivum* and its effect on peroxide catalytic activity and toxicology. J Chem. 2013; 2013:265864. https://doi.org/10.1155/2013/265864
15. Loza K, Heggen M, Epple M. Synthesis, structure, properties, and applications of bimetallic nanoparticles of noble metals. Adv Funct Mater. 2020; 1909260. https://doi.org/10.1002/adfm.201909260
16. Banadaki AD, Kajbafvala A. Recent advances in facile synthesis of bimetallic nanostructures: an overview. J Nanomater. 2014; 2014:985948. https://doi.org/10.1155/2014/985948
17. Nadhirah NA, Arham NA, Jai J, Hadi A. Plant Extract as Reducing Agent in Synthesis of Metallic Nanoparticles: A Review. Adv Mater Res. 2013; 832:350-355. https://doi.org/10.4028/www.scientific.net/AMR.832.350
18. Rostek A, Loza K, Heggen M, Epple M. X-ray powder diffraction to analyse bimetallic core-shell nanoparticles (gold and palladium; 7-8 nm). RSC Adv. 2019; 9(46):26628-26636. https://doi.org/10.1039/C9RA05117A
19. Esparza R, Téllez-Vázquez O, Ángeles-Pascual A, Pérez R. Synthesis and characterisation of bimetallic nanoparticles by Cs-corrected scanning transmission electron microscopy. Mater Charact. 2015; 105:35-42. https://doi.org/10.1007/978-3-319-15204-24
20. Rami JM, Patel CD, Patel CM, Patel MV. Thermogravimetric analysis (TGA) of some synthesised metal oxide nanoparticles. Mater Today Proc. 2021; 43:655-659. https://doi.org/10.5465/AMBPP.2021.14499abstract